



## Research article

## Mixed phytochemicals mediated synthesis of copper nanoparticles for anticancer and larvicidal applications



Gopalan Rajagopal<sup>a</sup>, Ambikapathi Nivetha<sup>b</sup>, Madasamy Sundar<sup>c</sup>, Theivendran Panneerselvam<sup>d</sup>, Sankaranarayanan Murugesan<sup>e</sup>, Pavadai Parasuraman<sup>f</sup>, Sattanathan Kumar<sup>g</sup>, Sakkanan Ilango<sup>a,\*,\*\*</sup>, Selvaraj Kunjiappan<sup>h,\*</sup>

<sup>a</sup> Postgraduate and Research Department of Zoology, Ayya Nadar Janaki Ammal College, Sivakasi, 626124, Tamil Nadu, India

<sup>b</sup> Department of Chemistry, Bharathiar University, Coimbatore, 641046, Tamil Nadu, India

<sup>c</sup> Centre for Research and Postgraduate Studies in Botany, Ayya Nadar Janaki Ammal College, Sivakasi, 626124, Tamil Nadu, India

<sup>d</sup> Department of Pharmaceutical Chemistry, Swamy Vivekanadha College of Pharmacy, Elayampalayam, Tiruchengodu, 637205, Tamil Nadu, India

<sup>e</sup> Department of Pharmacy, Birla Institute of Technology & Science Pilani, Pilani Campus, Vidya Vihar, Pilani, 333031, Rajasthan, India

<sup>f</sup> Department of Pharmaceutical Chemistry, Faculty of Pharmacy, M.S. Ramaiah University of Applied Sciences, M S R Nagar, Bengaluru, 560054, Karnataka, India

<sup>g</sup> Department of Pharmaceutical Chemistry, Paavai College of Pharmacy and Research, Namakkal, 637018, Tamil Nadu, India

<sup>h</sup> Department of Biotechnology, Kalasalingam Academy of Research and Education, Krishnankoil, 626126, Tamil Nadu, India

## ARTICLE INFO

## Keywords:

*Wrightia tinctoria* R.Br

GC-MS

Copper nanoparticles

Anticancer activity

Larvicidal activity

Molecular docking and hemolytic assay

## ABSTRACT

The synthesis of copper nanoparticles (CuNPs) using *Wrightia tinctoria* (Wt) R.Br extract is defined in this article as being convenient, environmentally friendly, and non-toxic. UV-visible spectrophotometry, FT-IR, XRD, particle size analyser, SEM-EDAX and TEM methods were used to describe the physicochemical properties of Wt extract mediated synthesized CuNPs (Wt-CuNPs). The Wt-CuNPs synthesized was found to be monodispersed and spherical, with an average size of 15 nm. Gas chromatography and mass spectrometry (GC-MS) research revealed that the Wt R.Br plant extract contains various phytochemical compounds. The properties of Wt-CuNPs were verified by the findings of characterization tests. Via *in silico* molecular docking experiments with established targets, the underlying mechanisms of cytotoxicity against breast cancer and larvicidal behaviour against *Aedes aegypti* of Wt-CuNPs were investigated. Interestingly, *in vitro* cytotoxicity studies showed 50% cell death (IC<sub>50</sub>) of Wt-CuNPs treated MCF-7 cells and Vero Cells (Kidney epithelial cells) were displayed at 119.23 µg.mL<sup>-1</sup> and 898.75 µg.mL<sup>-1</sup>, respectively. Also, Wt-CuNPs showed least LC<sub>50</sub> and LC<sub>90</sub> values for larvicidal activity against *A. aegypti* were of 32.10 µg.mL<sup>-1</sup> and 21.70 µg.mL<sup>-1</sup>, respectively. Furthermore, Wt-CuNPs is found to be less toxic and biocompatible in haemolytic assays. The findings clearly showed that biosynthesized Wt-CuNPs have been used as a possible anticancer and larvicidal agent, as well as being environmentally friendly.

## 1. Introduction

Nanotechnology is now one of the most dynamic areas of study in materials science, biomedical science, and medicine [1, 2]. Metallic nanoparticles are multifunctional and have been used in a variety of industries and medical applications, including medication distribution, cancer treatment, wastewater treatment, and DNA research, as antibacterial agents and biosensors, as well as solar power generation and catalysis. Green synthesis of metallic nanoparticles has been suggested as a cost-effective and environmentally friendly solution to chemical and

physical methods. Copper nanoparticles (CuNPs) have piqued researchers' attention in recent years owing to their applications in industry and medicine [3, 4].

Biosynthesis of metal oxide nanomaterials utilizing different parts of plant extract, such as leaves, stem, core, and flower, has been found to be the most effective process. Plant extracts contain a number of phytochemical compounds that serve as metal oxide nanoparticle reducers and stabilizers. Furthermore, the synthesis of nanoparticles using phytochemical compounds is environmentally friendly, non-toxic, inexpensive, and simple to do at room temperature [5]. Moreover, it will help to

\* Corresponding author.

\*\* Corresponding author.

E-mail addresses: [silangosakkanan@gmail.com](mailto:silangosakkanan@gmail.com) (S. Ilango), [selvaraj.k@klu.ac.in](mailto:selvaraj.k@klu.ac.in) (S. Kunjiappan).

<https://doi.org/10.1016/j.heliyon.2021.e07360>

Received 25 April 2021; Received in revised form 16 May 2021; Accepted 17 June 2021

2405-8440/© 2021 Published by Elsevier Ltd. This is an open access article under the CC BY-NC-ND license (<http://creativecommons.org/licenses/by-nc-nd/4.0/>).

diminish the consequences of damage caused to the environment by artificial materials and methods [6, 7].

Green mediated synthesized metal oxide nanoparticles may target and arrest the proliferation of variety of cancer cells. Among the various metal oxide nanoparticles (e.g., TiO<sub>2</sub>, ZnO, Fe<sub>3</sub>O<sub>4</sub>, Fe<sub>2</sub>O<sub>3</sub>), copper oxide (CuO) nanoparticles are considered as economically viable and showed promising anticancer activity. As compared to other metal oxide nanoparticles, CuONPs cause higher DNA damage and oxidative stress in human epithelial cancer cells [8]. Recently, researchers focused on the CuONPs coated with plant derived bioactive compounds for the prevention of mosquito-borne illness with less or nil toxicity [9, 10]. In the past, the crude extract of the plant was used for larvicidal activity [11].

Green NPs have been synthesized using different plant sections or whole plants due to the abundance of bioactive compounds in plants. This method has been effective by using a plant extract. The *Punica granatum* peel [12], *Ziziphus spina-christi* (L.) Wild fruit [13], *Asparagus adscendens* Roxb. root and leaf [14], *Eclipta prostrata* leaf [15] and *Ginkgo biloba* Linn leaf [16] have all been used to effectively synthesize CuNPs.

*Wt* R.Br is a herbal plant whose bark is used to relieve stomach discomfort, skin infections, and wounds, as well as acting as a snake venom treatment. Antipyretic, anti-diarrheal, and anti-hemorrhagic properties are also present. This plant's seeds are known as aphrodisiacs, and its leaves are used to treat toothaches. Anti-inflammatory agents are present in the plant content [17]. The current research focuses on the synthesis of copper nanoparticles from *Wt* R.Br, as well as their characterization and biological applications, which involve anticancer and larvicidal properties.

## 2. Experimental section

### 2.1. Materials

HiMedia Laboratories, Mumbai, India, given copper (II) sulfate pentahydrate (CuSO<sub>4</sub>·5H<sub>2</sub>O), sodium borohydride (NaBH<sub>4</sub>), Thiazolyl Blue Tetrazolium Bromide, and HPLC grade water. Biological reagents for cell culture studies were purchased from Gibco, Bengaluru, India, including Dulbecco's enhanced Eagle's medium (DMEM) with 4.5 g/L glucose, 4.0 mM L-glutamine and sodium pyruvate, Penicillin/Streptomycin (10,000 U/mL), fetal bovine serum (FBS), 0.25 percent Trypsin-EDTA (1X), and Phosphate buffers.

### 2.2. Plant materials

In the month of May 2019, the leaves of *Wt* R.Br were collected from the Western Ghats, Srivilliputtur (latitude: 9.5161°N and longitude: 77.63°E), Virudhunagar Dist. Tamilnadu, India. Taxonomists at the Centre for Research and Postgraduate Studies in Botany, Ayya Nadar Janaki Ammal College, Sivakasi, Tamilnadu, India, verified the plant organisms.

### 2.3. *Wt* leaf extract preparation

The *Wt* leaves were washed systematically with de-ionized water 3–4 times in order to remove the dust particles and were subjected to air-drying under dark condition for nearly 3–5 days. Then, dried leaves were grounded into fine powder (140 mesh size approximately) using pulveriser machine. Accurately weighed 5 g of fine leaf powder was taken for extraction, and placed in a beaker containing 100 mL of Milli-Q water. Then, it was boiled at 60 °C for 30 min. The color of the aqueous solution was altered from watery green to light brown. Then after, the extract was kept in a room temperature (~35 °C) for 30 min for cooling, and extract was filtered through filter paper (Whatman No.1). For further studies and subsequent examination, the filtered extract was preserved at -20 °C.

### 2.4. Gas chromatography-mass spectrometry for phytochemical analysis

The leaf extract of *Wt* was analyzed using a GC-MS method (GC/MS-series QP2010, Shimadzu, Tokyo, Japan) and a Thermal Desorption (TD) system. An Rtx-5 capillary column (30 m × 0.25 mm; film thickness of 0.25 μm) was used in the GC-MS, with helium as the carrier gas at a steady flow rate of 1.21 mL/min. The oven temperature was initially set at 60 °C, then raised at a rate of 5 °C/min to 200 °C, accompanied by a final rise to 280 °C. The scan was done with a m/z range of 50–650. The mass spectrometer was set to 70 eV, and the NIST library was used to identify mass fragmentation trends of individual phytochemical compounds [18].

### 2.5. Synthesis of CuNPs

Environmental benign synthesis of CuNPs by using plant extracts [19]. In brief, accurately weighed 0.49 g of CuSO<sub>4</sub>·5H<sub>2</sub>O was liquefied in 20 mL of de-ionised water and stirring was continued for 30 min under magnetic stirrer until clear liquid was achieved. To the above solution, 20 mL of *Wt* extract was added and stirred for another 3 h. The colour changed to black from pale green was observed. Aqueous ammonia solution was used as precipitating agent and also used to maintain the pH of the reaction. After that, water and ethanol were used to wash the precipitated CuNPs, then the precipitate was dried at 60 °C.

### 2.6. Characterization of CuNPs

The bio-reduction of copper sulphate ions by *Wt* leaf extract was monitored by UV-1601 Shimadzu spectrophotometer at a resolution of 1 nm, wavelength range of 400 and 800 nm. The *Wt*-CuNPs and ethanol were mixed together and made it as thin film on a glass substrate and measured by Ultima IV - Rigaku diffractometer with Cu K $\alpha$  radiation ( $\lambda$  = 1.540 Å, 45 kV & 30 mA). FT-IR measurement was done by using FTIR-8400S-spectrophotometer (Shimadzu, International, Co. Ltd, Tokyo, Japan) to determine the different types of chemical bonds between bioactive compounds of *Wt* and copper sulphate solution. Samples were scanned from 400–4000 cm<sup>-1</sup> with potassium bromide pellets. Representative peaks of *Wt*-CuNPs are expressed in a reciprocal wavelength (cm<sup>-1</sup>). Photon correlation spectroscopy (PCS) was used to determine the mean particle size (Z-average) of freshly synthesized *Wt*-CuNPs using Shimadzu SALD-2300 (WingSALD II: version 3.1.1) instruments. All measurements were performed at 25 °C at a detection angle of 90°. The topographic nature of *Wt*-CuNPs was examined by SEM. The *Wt*-CuNPs were uniformly spreaded, sputter-coated with platinum using an ion coater for 120s, and then visualized under SEM EVO18-CARL ZEISS, USA. Energy Dispersive X-ray (EDX) spectroscopy (a part of SEM which was done by using Quantax 200 with X Flash® 6130) used for detecting the arrangement of elements in the analyte sample. TEM analysis was carried out by TEM - JEOL-2100 at magnification of 46000 $\times$ . Freshly synthesised *Wt*-Cu NPs (~0.5 mL) was spraying onto a formvar resin-coated TEM grid and air-dried up to 10 min earlier, then the morphology of *Wt*-CuNPs was photographed.

### 2.7. Copper ion release study

Copper is a trace element that is considered vital elements for human health but it are dangerous at high concentrations. Here, a copper ions release from synthesized *Wt*-CuNPs was estimated by using Atomic Absorption Spectrophotometer (PerkinElmer, Analyst spectra 200 AAS) with certified standards by AOAC method [20]. It was equipped with a copper hollow cathode lamp and air-acetylene burner. The instrumental parameters were as follows: wavelength 324.8 nm, lamp current 3 mA, bandpass 0.5 nm. A specified amount (1 mg) of freshly synthesized *Wt*-CuNPs was mixed with 5 mL de-ionized water and kept at room temperature for 24, 48, and 72 h. After 24, 48 and 72h, the *Wt*-CuNPs was removed from de-ionized water by ultracentrifuge at 10,000 rpm for 10 min. Later, the de-ionized water was undergoing AAPS by measuring the

concentration of Cu ions. The standard solution of 1000 mg mL<sup>-1</sup> copper was prepared by dissolving 0.6706 g of CuCl<sub>2</sub>·2H<sub>2</sub>O (Sigma, Bengaluru) in de-ionized water, adding 2 mL of concentrated nitric acid (Sigma, Bengaluru; 70%, d = .42), and diluting to 250 mL in a volumetric flask. The required concentration of copper solution was prepared by appropriate dilution of the stock solution.

### 2.8. *In silico* molecular docking studies

Recently, *in silico* molecular docking technique is a key tool in structural biology mainly utilized for computer aided drug design. The techniques aid to predict the best binding mode of a small molecule (e.g. drug and enzyme or protein) to a targeted macromolecule. The 3D molecular structure of identified phytochemicals (ligands) from *Wt* leaf extract was built by using Chem Draw Ultra 8.0, and ligand optimization was performed by using Chemistry at Harvard Molecular Mechanics (CHARMm) force field by energy minimization protocol. The built structures were converted to.pdb file format using BIOVIA Discovery Studio Visualizer 4.0 software (Accelrys Software Inc., San Diego, CA). 3D structure of target Wnt/ $\beta$ -catenin (PDB ID: 1JDH) [21] and gustatory receptor of *A. aegypti* (PDB ID: 2LPV) [22] was obtained from RCSB Protein Data Bank (PDB). Prior to analysis, the protein was cleaned and missed residues were added using the prepare protein protocol present on Swiss-Pdb Viewer v4.1.0. The files were saved as target.pdb. Using PyRx software, polar hydrogen atoms and Kollman partial charges were added to the 3D structures. The macromolecule file was changed as.pdbqt file format for further analysis. The active site of the target protein was selected based on bounded co-crystal ligand present in the protein structure. The bounded ligand molecule interacted region was considered an active site for further docking calculation [23].

### 2.9. Molecular dynamics (MD)

The molecular dynamics simulation was investigated to determine the binding stability, confirmation and interaction modes between the selected phytochemical compounds (ligand) with target proteins (Wnt/ $\beta$ -catenin of cancer and gustatory receptor of *A. aegypti*) [24]. The time-dependent modification of the complexes were calculated over 100 ns using Desmond dynamic package 2017 in Schrödinger (Academic version) under Linux environment [25]. The OPLS (optimized potentials for liquid simulations)-2005 force field was applied for preparing the complex of identified phytochemicals with the Wnt/ $\beta$ -catenin and gustatory receptors [26]. Further, a water model was built at the distances of 10 Å units of orthorhombic periodic boundary using the predefined SPC water model [27]. Moreover, by adding the specified number of counter ions, the electric charges were neutralized, and before the MD simulation process started, the system minimized their energies by heating and equilibrium processes. The final production step of the system continued up to 100 ns, at time steps of 0.001 ps; 300 K temperature and one atmospheric pressure (1.01325 bar), applied using the Nose-Hoover method with the NPT (isothermal-isobaric) ensemble [28, 29]. Appertaining to the interactions and dynamical properties of the complex, the finest confirmations were selected [30].

### 2.10. Anticancer activity

The cytotoxic potential of *Wt*-CuNPs performed against (MCF-7) human breast cancer and normal (Vero) cell lines by 3-(4,5-dimethylthiazol-2-yl)-2,5-diphenyl tetrazolium bromide (MTT) based rapid colorimetric assay [31]. For screening, the MCF-7 cells were seeded in a 96-well plate in 100  $\mu$ L of medium containing 5% FBS, at plating density 10,000 cells/well and incubated at 37 °C, 5% CO<sub>2</sub>, 95% air and relative humidity (100%) for 48 h prior to addition of *Wt*-Cu NPs. After 48 h, different concentrations *Wt*-Cu NPs were added and incubated at 37 °C, 5% CO<sub>2</sub>, 95% air and relative humidity (100%) for 48 h. At the end of incubation time, 100  $\mu$ L (5 mg mL<sup>-1</sup>) of 0.5% MTT solubilized in

serum-free medium was added to each well and incubated for 4 h at 37 °C. MTT fixative solution (isopropanol with 0.04M HCl) of 100  $\mu$ L was added to the medium and removed after 4 h. ELISA plate reader (Bio-Rad, Model 680, Hercules, CA) was used to monitor the absorbance at 570 nm for viable cells. Triplicate was kept and the medium containing without the sample was served as control. The percentage of cell viability was calculated using the following Eq. (1):

$$\text{Cell viability (\%)} = \frac{A_t}{A_c} \times 100 \quad (1)$$

where,  $A_t$  and  $A_c$  are the mean absorbance of Cu NPs treated and control cells, respectively (n = 3).

### 2.11. Mosquito rearing

The *A. aegypti* eggs were collected from the unit of Vector Control Research Centre, Madurai, and maintained at our laboratory. The larvae were reared in enamel trays which contain chlorine free water. The larval feed is powdered dog biscuits and dry yeast in the ratio of 3:1. Then, larvae were allowed to grow until becomes 3<sup>rd</sup> instar stages, and they were used further in the determination of larvicidal activity [32].

### 2.12. Larvicidal activity

Different concentrations of plant extract and *Wt*-CuNPs were prepared in 100 mL de-ionized water. Bioassay of the target larvae to varying concentrations of plant extract and synthesized *Wt*-CuNPs was performed as per the reported procedure with slight modifications [33]. Around 25 larvae were treated to each test at different concentration. Similarly, each test included a control group (distilled water) with three replicates. The death was noted after 48 h of treatment followed to slightly modified method of WHO [34]. The Larval mortality range was determined by Probit analysis of Finney method using SPSS Package (v16.0).

### 2.13. Hemolytic assay

The hemolytic activity of *Wt*-CuNPs, determined in fresh anti-coagulated human blood cells. The cells were washed twice with phosphate buffered saline (PBS), and diluted at 10% in concentration, 800  $\mu$ L of nanoparticles diluted at the concentrations of 100, 50, 25, 12.5, 6.25, 3.12, 1.56, 0.78  $\mu$ g.mL<sup>-1</sup> in phosphate buffered saline solution at micro-centrifuge tubes. Negative control as PBS and positive control 1% Triton X-100, 200  $\mu$ L of Red Blood Cell (RBC) suspension added all tubes incubated for 1 h at 37 °C. All treated tubes centrifuged at 2000 rpm for 5 min and supernatants were transferred to new 96 well micro-titer test plate, and absorbance was read at 540 nm. The amount of hemoglobin released was calculated (Eq. n:(2)) using negative control (no hemolysis) and Triton X-100 (positive control, complete hemolysis) [34].

$$\% \text{ of hemolysis} = \frac{AS - AN}{AP - AN} \times 100 \quad (2)$$

where, AS = Abs of sample treated, AP = Abs of positive and AN = Abs of Negative control respectively.

## 3. Results and discussion

The GC-MS spectra of *Wt* R.Br leaf extract showed 26 substances, 17 of which were known as phytochemicals and the others were unidentified (Figure 1). The presence of phytochemical compounds was verified by comparing retention time, mass spectra, and a library of regular compounds. Table 1 shows the substances discovered and their structures. In the 'experiment,' the phytosynthesis of CuNPs from *Wt* R.Br leaf extract was initially verified by colour transformation from pale yellow to dark colour (Figure 2), while no colour transition was detected

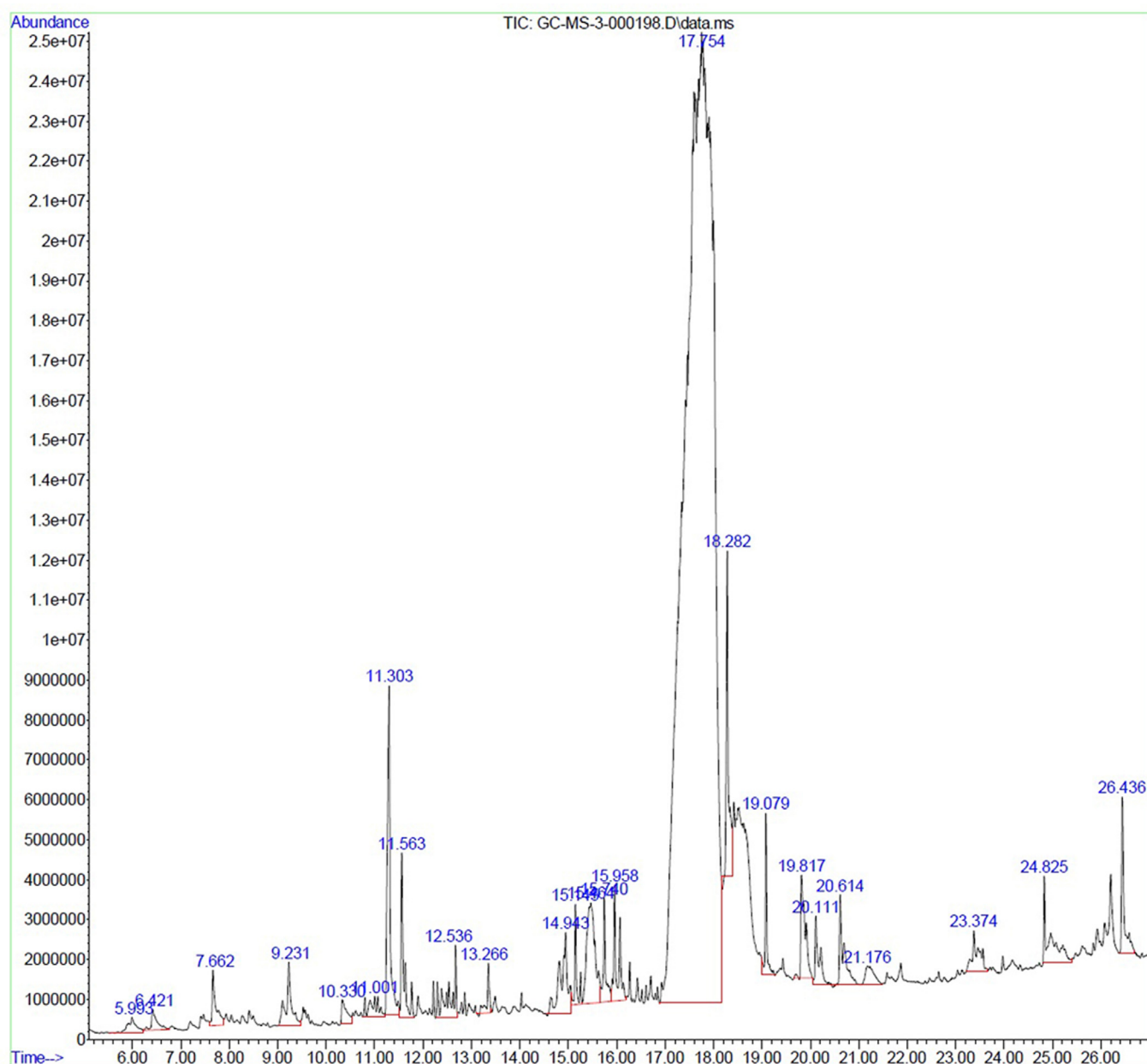


Figure 1. GC-MS spectra of *Wrightia tinctoria* R.Br plant extract.

in the 'control' setup. Similar to these changes were observed in the green synthesis of CuONPs from *A. lebbek* leaf extract [35]. The *Wt*, acts as a reducing agent of Cu NPs and a colour change of dark brown within 30 min of incubation confirms the formation of CuONPs [36, 37].

### 3.1. UV-visible spectral analysis

An Ultraviolet–Visible spectrum is used to analyse the Surface Plasmon Resonance (SPR) of nanoparticles. The UV-Visible spectra for CuNPs were in the range of 250 nm–360 nm [38, 39]. Likewise, our CuNPs synthesized using *Wt* R.Br showed absorption peak maxima at 357 nm in the UV–Visible spectra (Figure 3). On account of SPR excitation in CuNPs, the colour change occurs [40, 41]. According to Mei's theory, if the single peak was obtained in UV-Visible spectrum, it confirms that the nature of the synthesized nanoparticle is spherical shape [42], and obtained single peak confirmed that *Wt*-Cu NPs were spherical shape. Previous studies also revealed that the single peak confirms the spherical shape of CuNPs [35].

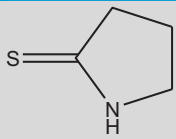
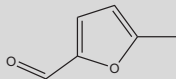
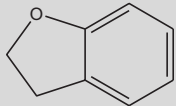
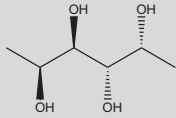
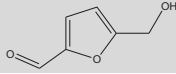

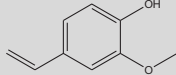
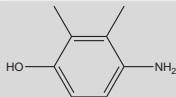
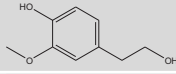
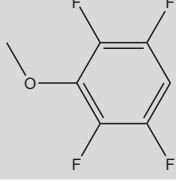
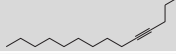
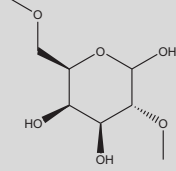

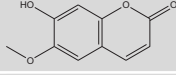
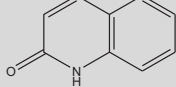
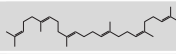
### 3.2. Scanning Electron Microscope (SEM) analysis

In biological applications, functional properties such as the morphological form and scale of nanoparticles play a significant role in evaluating cancer cell permeation and disease vector regulation. SEM analysis was employed to determine the particle size and morphology of the green synthesized *Wt*-CuNPs. SEM images of CuNPs are shown in Figure 4 (a) and (b). The surface morphology was highly influenced by the plant leaf extract which was used as fuel. From the SEM analysis, the mean particle sizes of the synthesized nanoparticles were found to be 29–37 nm. The *Wt*-CuNPs are monodispersed and highly stable, according to SEM results. CuNPs have morphological configurations that include triangles, pentagons, and hexagons [42, 43].

### 3.3. Energy Dispersive X-ray analysis (EDAX)

The composition of the element present in the particle, atomic and weight percentage was determined for *Wt*-Cu NPs by EDAX analysis.

**Table 1.** Analysed phytochemicals from extract of *Wrightia tinctoria* R.Br.

S. No	Retention time	% Area of peak	Compound analysed	Molecular formula	Molecular weight (in g/mol)	Mass (in g/mol)	Structure
1	5.993	0.35	2-Pyrrolidinethione	C <sub>4</sub> H <sub>7</sub> NS	101.17	101.03	
2	6.421	0.32	2-Furancarboxaldehyde, 5-methyl-	C <sub>6</sub> H <sub>6</sub> O <sub>2</sub>	110.111	110.04	
3	10.330	0.33	Benzofuran, 2,3-dihydro-	C <sub>8</sub> H <sub>8</sub> O	120.15	120.06	
4	11.001	0.47	1,6-Dideoxygalactitol	C <sub>6</sub> H <sub>14</sub> O <sub>4</sub>	150.17	150.09	
5	11.303	2.53	5-Hydroxymethylfurfural	C <sub>6</sub> H <sub>6</sub> O <sub>3</sub>	126.11	126.03	
6	11.303	2.53	4-Mercaptophenol	C <sub>6</sub> H <sub>6</sub> OS	126.18	126.01	
7	11.563	1.15	2-Methoxy-4-vinylphenol	C <sub>9</sub> H <sub>10</sub> O <sub>2</sub>	150.17	150.07	
8	14.943	1.53	4-Amino-2,3-xyleneol	C <sub>8</sub> H <sub>11</sub> NO	137.18	137.08	
9	14.943	1.53	Homovanillyl alcohol	C <sub>9</sub> H <sub>12</sub> O <sub>3</sub>	168.19	168.08	
10	15.145	0.5	2,3,5,6-Tetrafluoroanisole	C <sub>7</sub> H <sub>4</sub> F <sub>4</sub> O	180.1	180.02	
11	15.740	0.68	4-Tetradecyne	C <sub>14</sub> H <sub>28</sub>	196.37	194.2	
12	17.754	0.77	2,6-Di-O-methyl-d-galactopyranose	C <sub>8</sub> H <sub>16</sub> O <sub>6</sub>	208.21	208.09	
13	19.079	0.69	Phytol	C <sub>20</sub> H <sub>40</sub> O	296.5	296.30	
14	20.614	0.99	Scopoletin	C <sub>10</sub> H <sub>8</sub> O <sub>4</sub>	192.16	192.04	
15	23.374	0.70	2(1H)-Quinolinone	C <sub>9</sub> H <sub>9</sub> NO	147.17	145.05	
16	24.825	1.16	Squalene	C <sub>30</sub> H <sub>50</sub>	410.73	410.39	

(continued on next page)



Table 1 (continued)

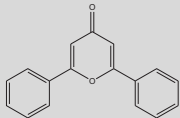
S. No	Retention time	% Area of peak	Compound analysed	Molecular formula	Molecular weight (in g/mol)	Mass (in g/mol)	Structure
17	26.50	1.06	4H-Pyran-4-one, 2,6-diphenyl	C <sub>17</sub> H <sub>12</sub> O <sub>2</sub>	248.27	248.08	



Figure 2. The colour changes from pale yellow to dark colour of *Wt*-CuNPs a)  $\text{CuSO}_4$  solution b) *Wrightia tinctoria* R.Br c) Synthesized *Wt*-CuNPs.

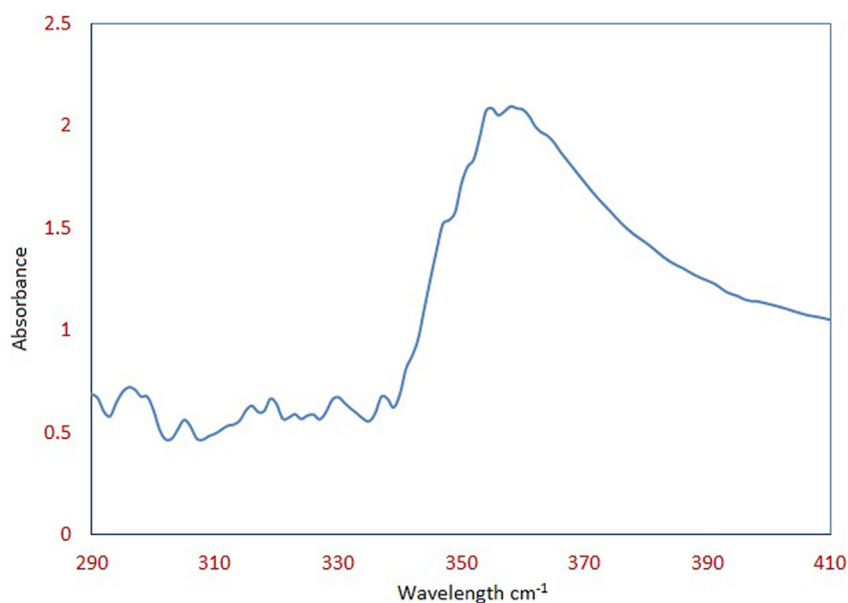


Figure 3. UV-Visible spectra of *Wt*-CuNPs at 357 nm.

Figure 4(c) reveals the EDX pattern of *Wt*-Cu NPs, which showed copper and oxygen atoms were present in the nanoparticles. This confirms the formation of Cu NPs. None of the peaks other than copper and oxygen was inferred from this analysis which showed that there were no impurities in the nanoparticles [43]. Similar observations were reported in green synthesized Cu NPs, and Cu NPs synthesized with sublimated precursors [44, 45].

### 3.4. Transmission Electron Microscope (TEM) analysis

TEM analysis was performed to know the morphological shape and size of the synthesized Cu NPs. From Figure 5(a), the particles are spherical in shape and size was approximately 15–40 nm. This result indicates that the synthesized Cu NPs were crystalline and

monodispersed. Selected area electron diffraction (SAED) pattern of Cu NPs were shown in Figure 5(b).

### 3.5. Fourier Transform-Infrared (FT-IR) analysis

Figure 6 showed the vibrational spectra of both *Wrightia tinctoria* R.Br plant extract and *Wt*-Cu NPs. The characteristic peak appeared at  $3404\text{ cm}^{-1}$  was attributed to water molecule present in the plant extract. The peak observed at  $2967\text{ cm}^{-1}$  allocated to  $-\text{C}-\text{H}$  group with stretching vibration. The  $2880$  and  $1750\text{ cm}^{-1}$  represents the presence of  $-\text{C}=\text{O}$  group in plant extract. The presence of  $-\text{N}-\text{H}$  group (stretching vibration) in plant extract was confirmed by the peak appeared at  $2313\text{ cm}^{-1}$ . The peak appeared at  $1644\text{ cm}^{-1}$  showed the presence of  $-\text{N}-\text{H}$  group (bending vibration) in plant extract. The peaks observed at  $1422$  and

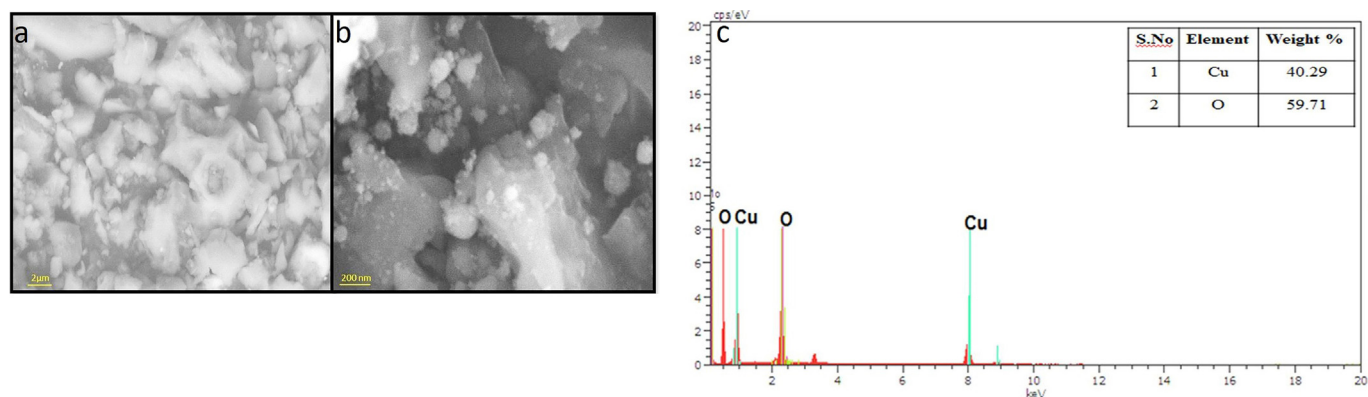


Figure 4. SEM analysis, (a) and (b) the mean particle sizes of *Wt*-CuNPs (c) EDX analysis of *Wt*-CuNPs.

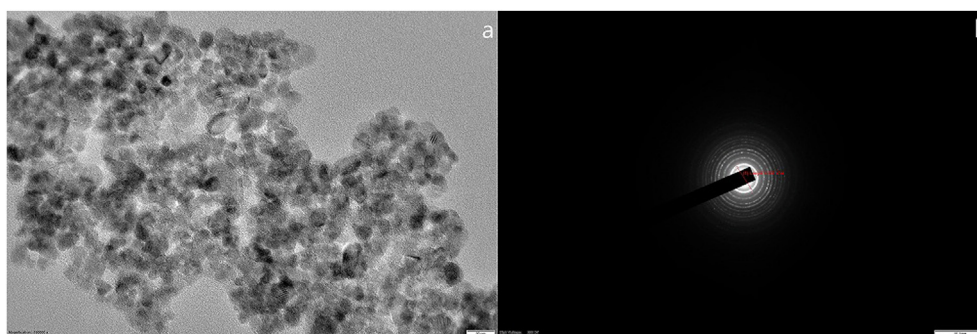


Figure 5. TEM micrograph of *Wt*-CuNPs (a); Selective Area Electron Diffraction (SAED) pattern (b).

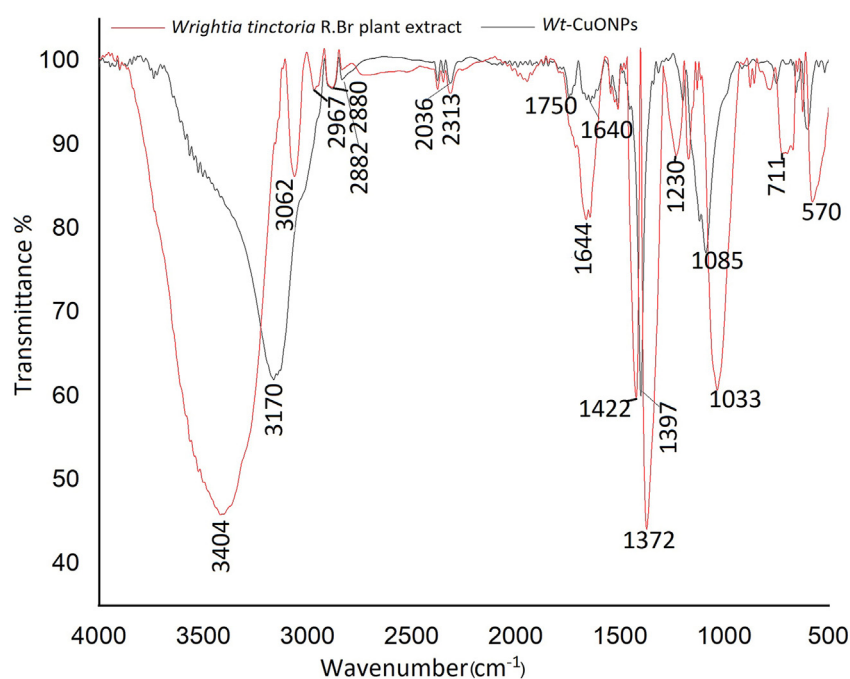


Figure 6. FTIR spectra of *Wrightia tinctoria* R.Br plant extract and synthesized *Wt*-CuNPs.

$1372\text{ cm}^{-1}$  indicate the  $-\text{C}-\text{H}$  group present in the plant molecule. The peak confirmed the secondary  $-\text{OH}$  functional group appeared at  $1230\text{ cm}^{-1}$  which is due to the bending vibration. The peak observed at  $711$  allocated to  $-\text{C}-\text{Cl}$  group with stretching vibration taken place in the plant molecule. The characteristic peak of for synthesized copper oxide nanoparticle was observed at  $570\text{ cm}^{-1}$ . The peak appeared at  $1640\text{ cm}^{-1}$

showed the presence of  $-\text{N}-\text{H}$  group (bending vibration) in the nanoparticle. The peak appeared at  $1397\text{ cm}^{-1}$  indicate the  $-\text{C}-\text{H}$  group present in the nanoparticle. The characteristic peak appeared at  $1085$  allocated to  $-\text{C}=\text{O}$  stretching vibration peak of Cu for synthesized copper oxide nanoparticle was observed at  $590\text{ cm}^{-1}$ . The stretching vibration at  $3428\text{ cm}^{-1}$  was assigned to water molecule while the band at  $1651\text{ cm}^{-1}$

was taken to be due to bending vibrations of  $\text{-C=O}$  group. The band at  $1416\text{ cm}^{-1}$  corresponds to the asymmetric stretching vibration of  $\text{-COO}^-$  group and band at  $1066\text{ cm}^{-1}$  were assigned to the  $\text{-C-O}$  stretching vibration. The existence of functional groups such as alcohol, amines, methyl amides, alkanes, halides, and aliphatic compounds proved that NPs were synthesized [7, 46, 47]. These functional groups act as biomolecules that stabilize, cap, and reduce NPs [48, 49].

### 3.6. X-ray Diffraction (XRD) studies

XRD was used to deduce the crystal structure and phase of the *Wt*-Cu NPs. A number of 2 $\theta$  peak intensities observed at  $31^\circ$ ,  $40.64^\circ$ ,  $41.73^\circ$  and  $50.28^\circ$  relating to 110, 111, 111 and 202 Bragg's appearance planes (Figure 7). The grain size can be calculated as 47.05 nm. All the peaks of Cu NPs can be indexed to the crystallographic parameters of a monoclinic crystal system Cu with the space group C2/c. The size of crystal under 100 nm suggested that the nanocrystalline nature of the biosynthesized Cu NPs was around 15 nm. Similar results were reported by other researchers from the structure analysis of XRD for biosynthesized Cu NPs [35, 37, 50, 51].

### 3.7. Particle size distribution

Dynamic light scattering (DLS) was used to determine the intensity-weighted mean diameter (Z-average) of the *Wt*-CuNPs, as seen in Figure 8. *Wt*-CuNPs had a diameter of 15 nm on average.

### 3.8. Copper ion release study

The concentration of Cu ions present in the samples after stipulated time periods presented in Figure 9. After 24 and 48 h there is no Cu ions released from *Wt*-CuNPs. While 72 h later, a negligible concentration of Cu ions released. The observed results clearly indicated that copper (II) sulfate pentahydrate ( $\text{CuSO}_4 \cdot 5\text{H}_2\text{O}$ ) completely converted into zero-valent copper nanoparticles, it is protected by *Wt* phytochemicals.

### 3.9. Molecular docking studies

The study exposed that molecular interaction and binding affinity of identified phytochemical compounds into selected target receptors (Wnt/ $\beta$ -catenin (PDB ID: 1JDH) and gustatory receptor of *Aedes aegypti* (PDB ID: 2LPV)) and that the ligands could be readily docked into the

possible binding site of the receptors. The potential strength of binding mode between ligand and protein is ascertained on the basis of scoring function and least binding energy. The results are summarised in Table 2. Among those docking result, the total value of binding energy ranged from  $-3.9$  to  $-7.1\text{ kcal.mol}^{-1}$  in 1JDH and  $-3.9$  to  $-7.5\text{ kcal.mol}^{-1}$  in 2LPV. In this range, the greatest result was observed in 4H-Pyran-4-one, 2,6-diphenyl of both receptors, which was minimal  $-7.1\text{ kcal.mol}^{-1}$  1JDH in and  $-7.5\text{ kcal.mol}^{-1}$  in 2LPV in term of total value. Figure 10 (a) and (b) represents the docking result of 4H-pyran-4-one, 2,6-diphenyl with target proteins (Wnt/ $\beta$ -catenin (PDB ID: 1JDH) and gustatory receptor of *Aedes aegypti* (PDB ID:2LPV)). Figure 10 (c) and (d) represents the interaction of amino acids at the active site of the target protein in the binding site. The binding involved in the formation of H-bonds was between the Wnt/ $\beta$ -catenin with ARG39, SER35 and gustatory receptor of *Aedes aegypti* with TYR83. On the basis of molecular docking studies, we proposed that the phytochemical compounds from *Wt* R.Br leaf extract might be a probable analogue for the development of anti-cancer and larvicidal agents.

### 3.10. Molecular dynamics

Molecular dynamics simulation can confirm the stability, evaluate the inter molecular interactions, and interactions between 4H-pyran-4-one, 2,6-diphenyl and the Wnt/ $\beta$ -catenin and the gustatory receptor complexes in a specific and artificial environment. Therefore, the study performed under the thermodynamical conditions (applied volume, density, pressure and temperature) for the time period of 100 ns, complex modifications were determined using the welding Desmond package. By applying ensembles, the complete system was annealed and equilibrated. Moreover, the structural modification of the complex was explored by the final production step. Next, to analyze the structural changes at each level, the trajectory complex was exposed to calculations of unique parameters such as root mean square deviation (RMSD), root mean square fluctuation (RMSF), conformational modification of ligands and intermolecular interactions of the 4H-pyran-4-one, 2,6-diphenyl and the Wnt/ $\beta$ -catenin and the gustatory receptor complexes. The RMSD of  $\text{C}\alpha$  protein atoms in this simulation was stabilized at  $3.1\text{ \AA}$  for 4H-pyran-4-one, 2,6-diphenyl and the Wnt/ $\beta$ -catenin complex (Figure 11(a)), and  $5.7\text{ \AA}$  for 4H-pyran-4-one, 2,6-diphenyl and the gustatory receptor complex (Figure 11(b)), indicating a stable conformation of the protein, which signifies that the molecules were profoundly steady during the MD simulation. In the mean function time, the fluctuation of the complex can

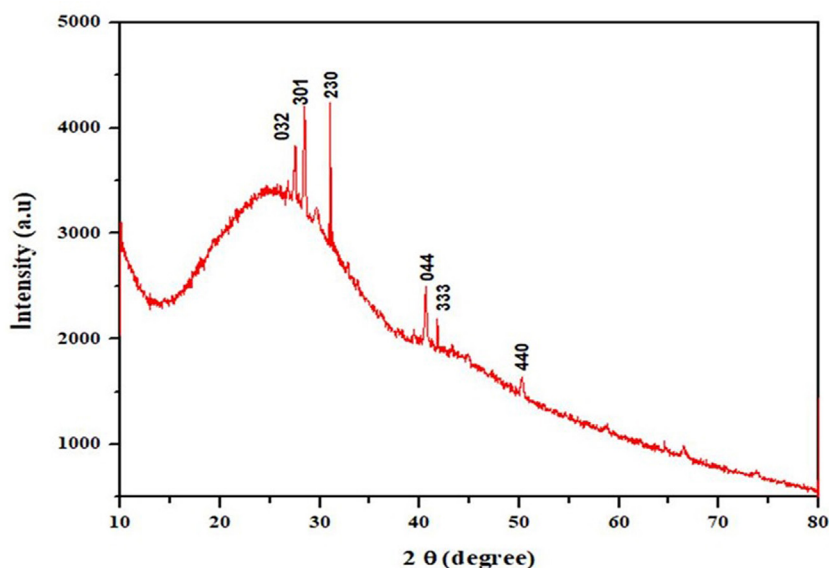


Figure 7. X-ray diffractogram of synthesized *Wt*-CuNPs.



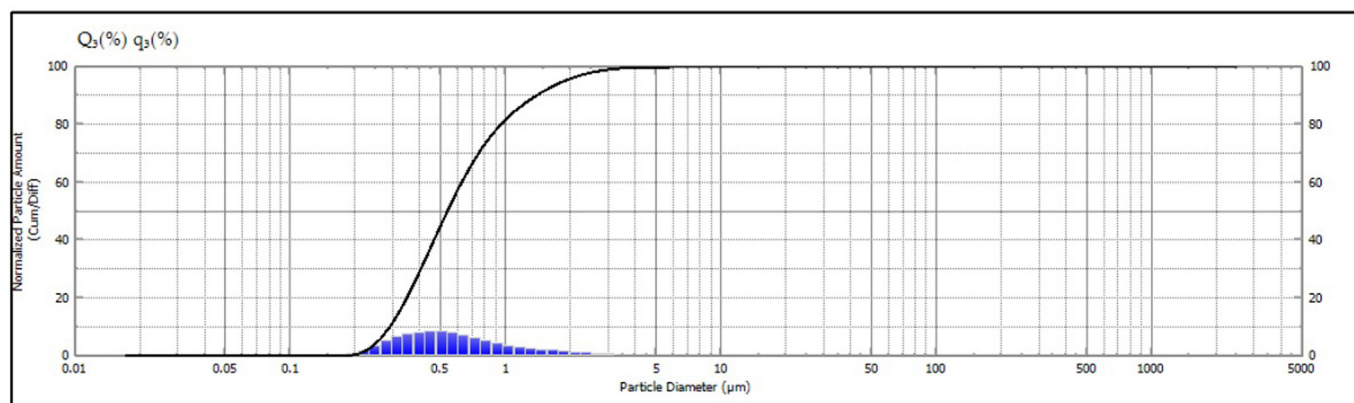


Figure 8. The DLS measurement of average particle size of *Wt*-CuNPs.

be investigated from the RMSF graph. Fluctuation was found in the residue index range of 85–95 at 4.7 Å for 4H-pyran-4-one, 2,6-diphenyl and the Wnt/ $\beta$ -catenin complex (Figure 11(c)), and 400 at 7 Å for 4H-pyran-4-one, 2,6-diphenyl (Figure 11(d)). Throughout the simulation, 4H-pyran-4-one, 2,6-diphenyl interacted with both receptors forming hydrogen bonds, hydrophobic interactions, ionic interactions, and water bridges. In case of 4H-pyran-4-one, 2,6-diphenyl and the Wnt/ $\beta$ -catenin complex: hydrogen bonding formed ILE57 was maintained consistently, with the multiple hydrophobic interactions, mild ionic interactions, and water bridges. Whereas, 4H-pyran-4-one, 2,6-diphenyl and the gustatory receptor complex: hydrogen bonding formed LYS345 was maintained consistently, with the strong hydrophobic interactions formed TRP383, mild ionic interactions, and water bridges. Interactions between the 4H-pyran-4-one, 2,6-diphenyl and the Wnt/ $\beta$ -catenin & gustatory receptors that occur more than 30.0% of the MD simulation time for the selected compound have also been presented in 2D format shown in Figure 11(e) and (f), respectively. We investigated the binding interaction of 4H-pyran-4-one, 2,6-diphenyl with Wnt/ $\beta$ -catenin & gustatory receptors. 4H-pyran-4-one, 2,6-diphenyl interaction with Wnt/ $\beta$ -catenin receptor, TRP 60, ILE57 and PHE37 amino acids of 100 ns (Figure 11(g)), In case of 4H-pyran-4-one, 2,6-diphenyl interaction with gustatory receptor LYS345 and TRP383 amino acids of 100 ns (Figure 11(h)).

### 3.11. Anticancer activity

Over the last two decades, copper-based compounds have had a strong biological impact, and copper, as one of the most important biological trace elements, plays a crucial role in anticancer agents [52, 53]. Nano ionization is a common modern strategy for overcoming this constraint, and it's also likely to be a targeted solution toward cancer cell growth. In the current study, the cytotoxic effect of *Wt*-CuNPs was evaluated against breast cancer cell line (MCF-7 cell lines) and the cytotoxicity to the normal (Vero) cell line was also studied. *Wt*-Cu NPs showed a cytotoxic effect on breast cancer cells in a dose-dependent manner. The  $IC_{50}$  values *Wt*-CuNPs against breast cancer cells were found 119.23  $\mu\text{g}\cdot\text{mL}^{-1}$  and 898.75  $\mu\text{g}\cdot\text{mL}^{-1}$  for Vero Cells (non-tumor cell) (Figure 12). *In vitro* cell viability assay clearly revealed that *Wt*-Cu NPs were severely toxic to human breast cancer cells even more than CuNPs (data not shown). Interestingly, the synthesized *Wt*-CuNPs had a lower cytotoxicity effect on Vero non-tumour derived cell line. The toxicity of CuNPs on cancer cells is mainly due to the release of copper ions from nanoparticles, which binds to the DNA of the cell. Thus, it causes damage in the DNA that leads to cell apoptosis [54].

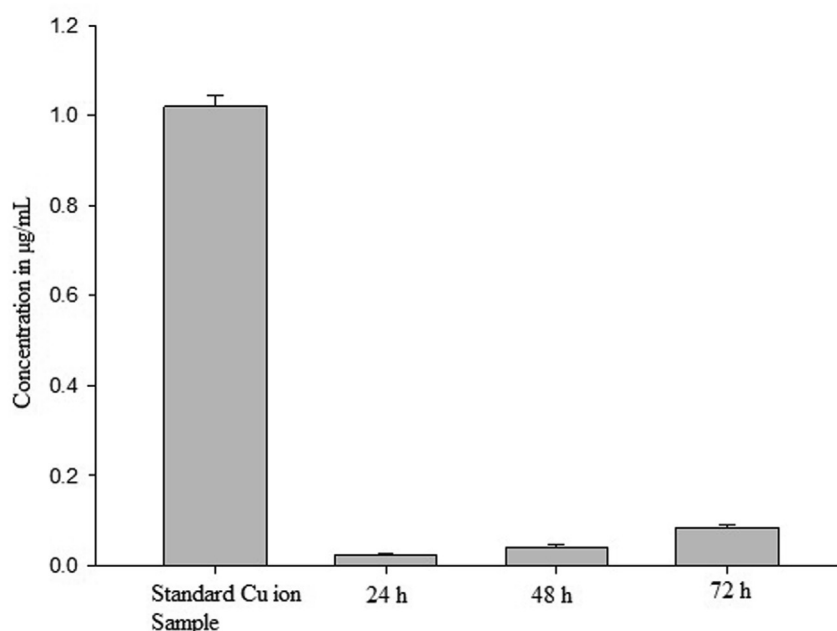


Figure 9. Copper ion released from *Wt*-CuNPs at different time interval. Values are mean  $\pm$  SD (experiments repeated 3 times).

**Table 2.** Shows the ligand-protein target and binding affinity.

Compounds	Gustatory receptor of <i>Aedes aegypti</i> (2lpv) binding affinity (kcal mol <sup>-1</sup> )	Wnt/ $\beta$ -catenin (1jdh) binding affinity (kcal mol <sup>-1</sup> )
2-Pyrrolidinethione	-3.9	-5.2
2-Furancarboxaldehyde, 5-methyl-	-3.4	-3.5
Benzofuran, 2,3-dihydro-	-3.8	-4.5
1,6-Dideoxygalactitol	-4.4	-5.1
5-Hydroxymethylfurfural	-4.1	-5
4-Mercaptophenol	-4.2	-4.8
2-Methoxy-4-vinylphenol	-3.9	-4.4
4-Amino-2,3-xyleneol	-4.8	-5
Homovanillyl alcohol	-4.4	-4.6
2,3,5,6-Tetrafluoroanisole	-4.6	-5.1
4-Tetradecyne	-4.4	-5.5
2,6-Di-O-methyl-d-galactopyranose	-5.4	-3.9
Phytol	-5.6	-6.2
Scopoletin	-6.3	-5.4
2(1H)-Quinolinone	-4.2	-4.3
Squalene	-5.3	-5.5
4H-Pyran-4-one, 2,6-diphenyl	-7.5	-7.1

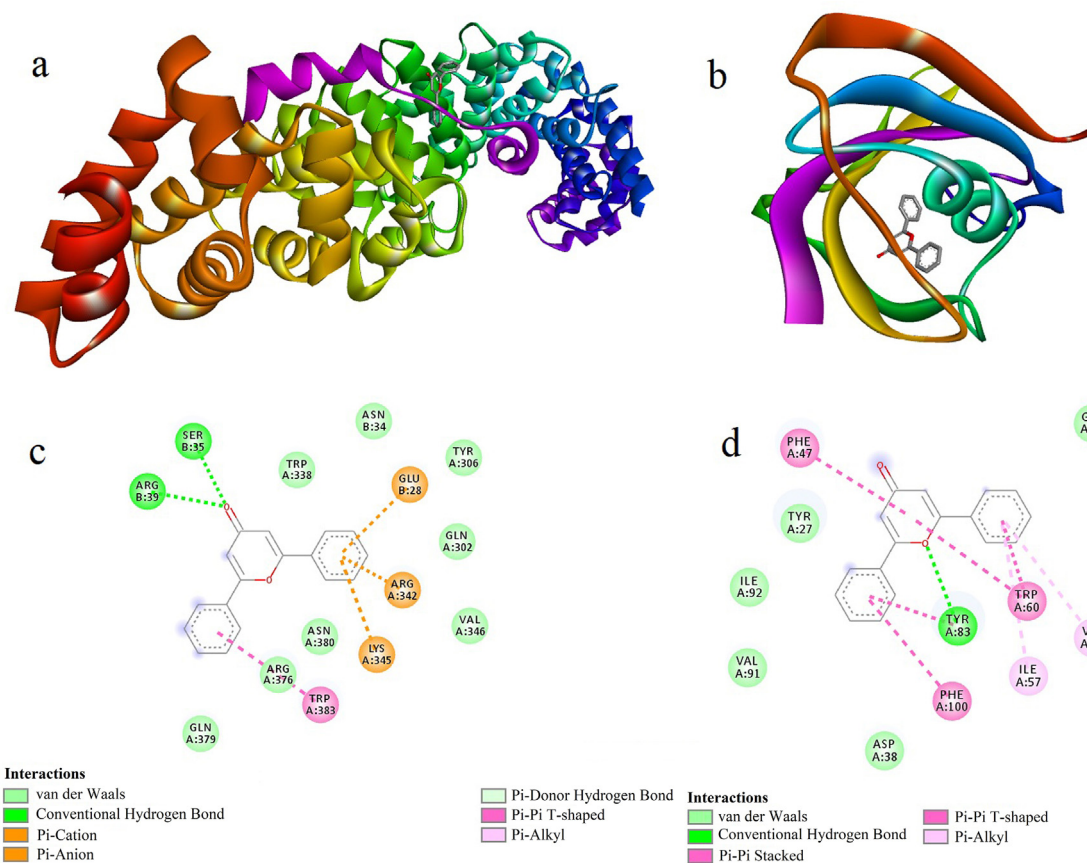
### 3.12. Larvicidal activity

Larval mortality improved with increase in the *Wt*-CuNPs concentration as compared to that of *Wt* R.Br leaf extract. The pure *Wt* R.Br leaf extract showed 24 h and 48 h LC<sub>50</sub> values of 183.32  $\mu\text{g.mL}^{-1}$  and LC<sub>90</sub>

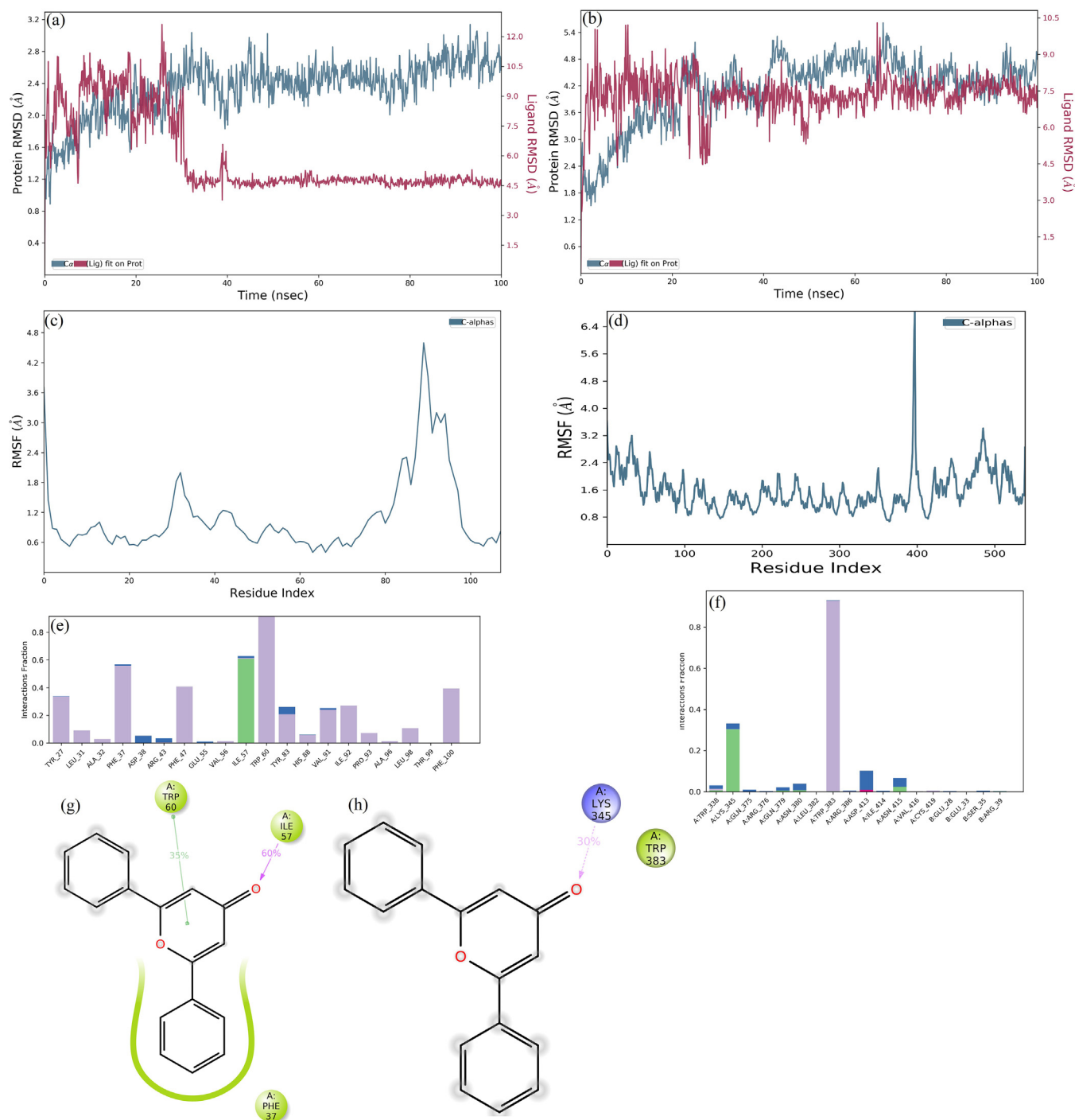
values 86.85  $\mu\text{g.mL}^{-1}$ , respectively against early III instar of *A. aegypti* (Table 3). While *Wt*-Cu NP showed 24 h and 48 h LC<sub>50</sub> values of 32.10  $\mu\text{g.mL}^{-1}$  and LC<sub>90</sub> values of 21.70  $\mu\text{g.mL}^{-1}$ , respectively against III instar of *A. aegypti* (Table 4). After treated, the larvae were observed under stereomicroscope 40 $\times$  magnification (Figure 13). Likewise, the green synthesized Cu NPs from *Tridax procumbens* leaf extract showed potent larvicidal activity of *A. aegypti* [55]. The toxicity mechanisms of mosquito mortality on treatment with nanoparticles treatment were studied recently. So, hypothetically suggested that the mechanism of toxicity against mosquito larval by the penetration of nanoparticle through the body. In intracellular space, nanoparticles degrade the enzymes and organelles, and it leads to the loss of cellular function and finally leads to cell death [55, 56]. The AgNPs from *Artemisia vulgaris* leaf extracts showed larvicidal activity. In the midgut of mosquito larvae, the nanoparticles will be accumulated and cause damage in the midgut, cortex region and epithelial cells. Similar to seaweed synthesized nanoparticles, many plant synthesized nanoparticles are also potent for mosquito larval control. The fruit pulp of *Cassia fistula*, *Nelumbo nucifera* and *Solanum tuberosum* synthesized AgNPs showed good larvicidal activity [57].

### 3.13. Hemolytic activity

At nanotoxicity range, the assessment on blood compatibility is more essential, because the blood cells are easily affected by nanoparticles platelet aggregation, coagulation, lymphocyte proliferation and the activation of complement system. The circulation of erythrocytes in the body passed through the cardiovascular system, which leads to defect in congenital malformation, DNA damage and cell membrane injury. An increase in percent hemolysis by more than 5%, according to the ASTM E2524-08 standard's hemolysis requirements, indicates that the



**Figure 10.** 3D interaction of 4H-pyran-4-one-2,6-diphenyl with target proteins Wnt/ $\beta$ -catenin (PDB ID: 1JDH) (a) Gustatory receptor of *Aedes aegypti* (PDB ID: 2LPV) (b) Interaction of amino acids at the active site binding pocket of the target protein (c) and (d).

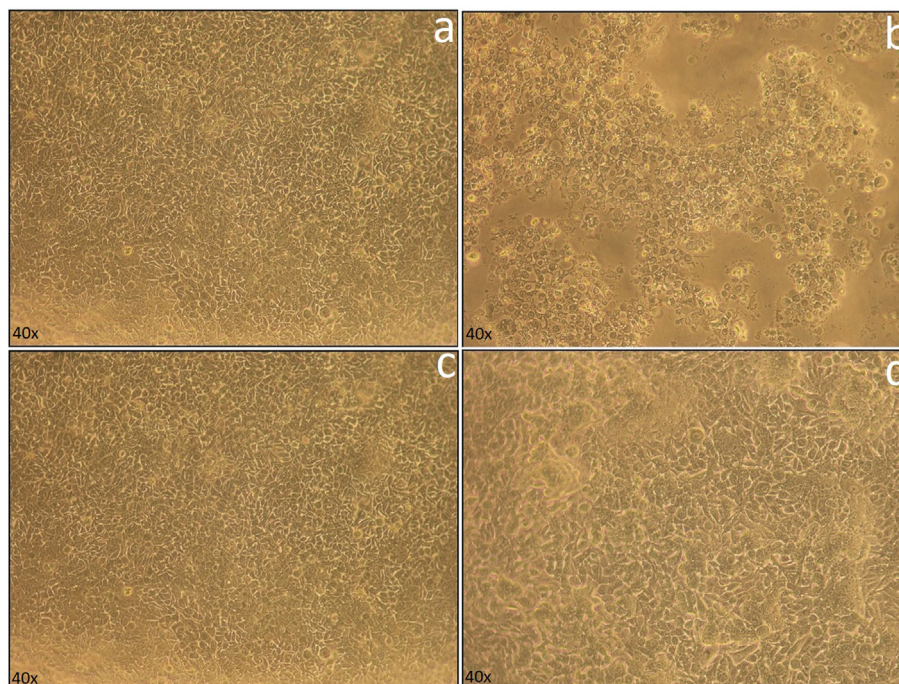


**Figure 11.** *4H*-pyran-4-one-2,6-diphenyl-Wnt/ $\beta$ -catenin RMSD (a); *4H*-pyran-4-one-2,6-diphenyl-gustatory receptor RMSD (b); *4H*-pyran-4-one-2,6-diphenyl-Wnt/ $\beta$ -catenin RMSF (c); *4H*-pyran-4-one-2,6-diphenyl-gustatory receptor RMSF (d); from MD simulation, *4H*-pyran-4-one-2,6-diphenyl-Wnt/ $\beta$ -catenin interaction (e); from MD simulation, *4H*-pyran-4-one-2,6-diphenyl-gustatory receptor (f); Intermolecular interactions between *4H*-pyran-4-one-2,6-diphenyl-Wnt/ $\beta$ -catenin interaction (g); Intermolecular interactions between *4H*-pyran-4-one-2,6-diphenyl-gustatory receptor.

research materials have induced harm to RBCs [58]. The ASTM E2524-08 normal criteria were not exceeded as compared to the baseline for hemolysis triggered by sample handling and processing. Although RBC harm was observed at nanoparticle concentrations greater than 10 mg/mL, as per the ASTM E2524-08 standard, it is essential to note that this dosage is equivalent to a human dose of 50 g nanoparticle for a 70 kg person [59]. The hemolytic activity of Wt-CuNPs was tested to determine the toxicity assessment in normal

human erythrocytes. The hemolytic analysis revealed that the increasing concentration increases the toxicity (Figure 14). In hemolysis, the red blood cells are contacted with water, and it is imperative to check this implant material before use. The permissible limit of haemolysis for biomedical materials should be less than 5% in all the cases [60]. The toxicity assessment by hemolytic assay revealed that Wt-CuNPs can be safe and also used for further investigation because it causes defect only at increased concentration.





**Figure 12.** The  $IC_{50}$  values of *Wt-Cu NPs* against breast cancer (MCF-7) and Vero (non-tumour) cell lines (a- MCF-7 Control, b- MCF-7 Treated, c- Vero Control, d- Vero Treated).

**Table 3.** 24 and 48 h larvicidal activity of *Wrightia tinctoria* R.Br leaf extract against 3<sup>rd</sup> instar of *A. aegypti*.

Exposure time (Hours)	Concentration ( $\mu\text{g.mL}^{-1}$ )	Mortality %	LC <sub>50</sub>	95% of LCL-UCL	LC <sub>90</sub>	95% of LCL-UCL	Intercept	X <sup>2</sup> Value	P Value	df - 3
24	60	22.26	183.32	142.00–225.79	390.32	317.74–572.65	-1.13	0.22	0.97	
	120	34.75								
	180	49.18								
	240	63.71								
	300	76.49								
48	60	41.93	86.85	19.78–122.82	255.88	213.55–345.81	-0.65	0.62	0.89	
	120	59.92								
	180	75.99								
	240	87.72								
	300	94.68								

LC- Lethal concentration, LCL - Lower confidential limit, UCL - Upper confidential limit, X<sup>2</sup> - Chi-square value.

**Table 4.** 24 and 48 h larvicidal activity of using green synthesized *Wt-CuONPs* against 3<sup>rd</sup> instar of *A. aegypti*.

Exposure time (Hours)	Concentration ( $\mu\text{g.mL}^{-1}$ )	Mortality %	LC <sub>50</sub>	95% of LCL-UCL	LC <sub>90</sub>	95% of LCL-UCL	Intercept	X <sup>2</sup> Value	P Value	df - 3
24	10	8.82	32.10	27.89–36.55	53.06	46.60–64.62	-1.96	0.37	0.94	
	20	22.96								
	30	44.88								
	40	68.54								
	50	86.30								
48	10	22.52	21.70	16.67–25.73	41.59	36.25–50.90	-1.39	0.57	0.90	
	20	45.62								
	30	70.34								
	40	88.08								

LC- Lethal concentration, LCL - Lower confidential limit, UCL - Upper confidential limit, X<sup>2</sup> - Chi-square value.

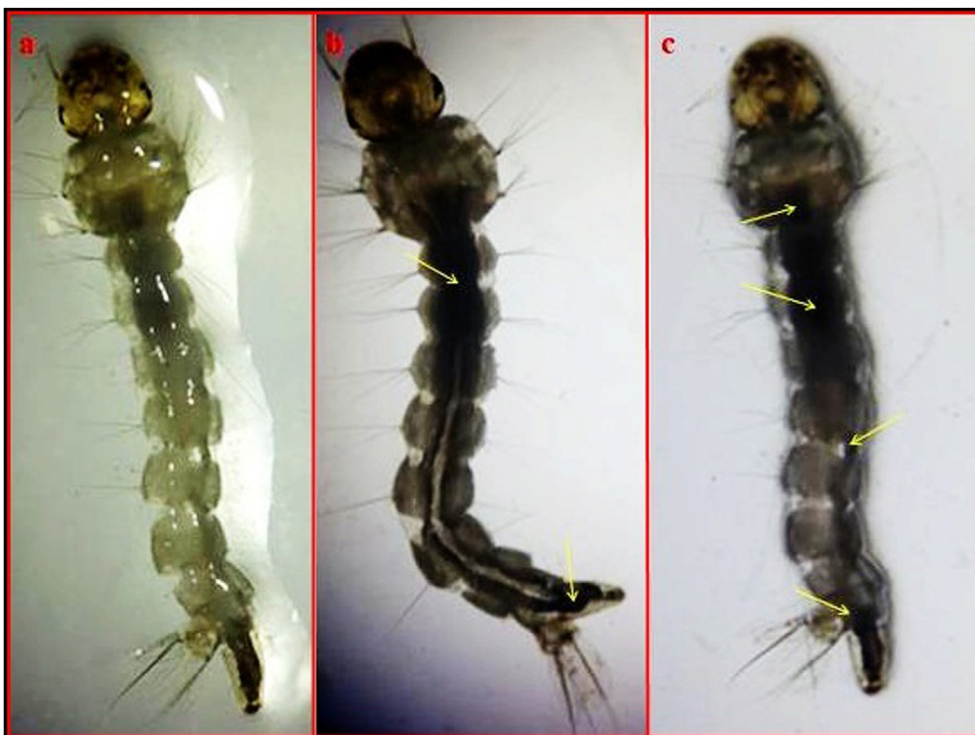


Figure 13. Stereo microscopic view of larvicidal activity of 3<sup>rd</sup> instar larvae of *A. Aegypti* (24 h) a) Control b) Crude extract c) *Wt*-CuNPs.

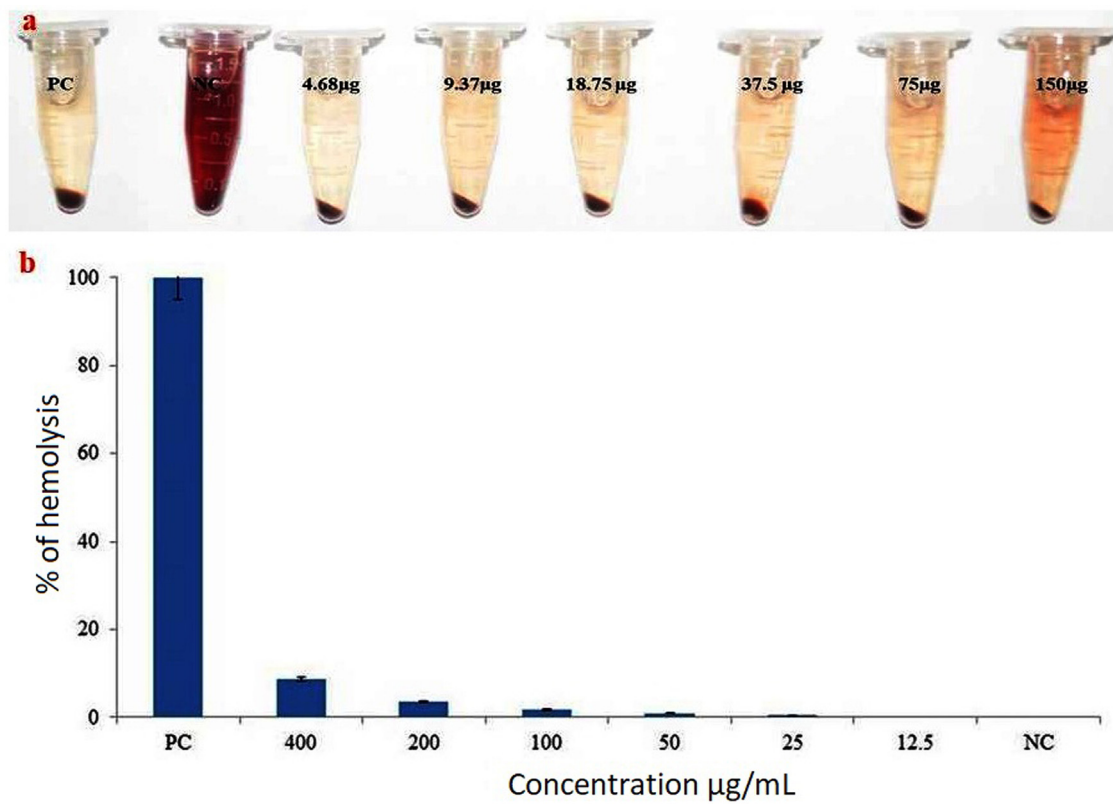


Figure 14. Toxicity assessment of *Wt*-CuNPs using haemolytic assay a) and b) at the increasing concentration.



#### 4. Conclusion

The potency of *Wt* R.Br extract-mediated CuNPs synthesis as an anticancer and larvicidal agent was revealed in this report, which demonstrated potent anticancer activity in MCF-7 cell lines. Also, *Wt*-CuNPs showed better larvicidal mortality against *A. aegypti* than the plant extract. *Wt* extract possess 17 potent phytochemical compounds, these were accumulated on the surface of CuNPs might have increased the bioavailability and effectively inhibited the growth of cancer cells. Further, the haemolytic analysis suggested that the synthesized *Wt*-CuNPs is eco-friendly. The analysis strategy would also pave the way for the discovery of additional CuNPs applications. However, in vivo experiments are required to further understand the process underlying anticancer behaviour and larvicidal exposure to *Wt* R.Br extract-mediated CuNPs.

#### Declarations

##### Author contribution statement

Gopalan Rajagopal; Ambikapathi Nivetha: Performed the experiments; Wrote the paper.

Madasamy Sundar; Pavadai Parasuraman; Sattanathan Kumar: Performed the experiments.

Theivendran Panneerselvam; Sankaranarayanan Murugesan: Analyzed and interpreted the data.

Sakkanan Ilango: Conceived and designed the experiments.

Selvaraj Kunjiappan: Conceived and designed the experiments; Wrote the paper.

##### Funding statement

This research did not receive any specific grant from funding agencies in the public, commercial, or not-for-profit sectors.

##### Data availability statement

No data was used for the research described in the article.

##### Declaration of interests statement

The authors declare no conflict of interest.

##### Additional information

No additional information is available for this paper.

#### Acknowledgements

The authors are grateful to the Management of Ayya Nadar Janaki Ammal College, Sivakasi, and Kalasalingam Academy of Research and Education, Krishnankoil, Tamilnadu, India, for utilizing research facilities.

#### References

- E.E. Elemike, I.M. Uzoh, D.C. Onwuide, O.O. Babalola, The role of nanotechnology in the fortification of plant nutrients and improvement of crop production, *Appl. Sci.* 9 (2019) 499.
- G. Rajagopal, A. Nivetha, S. Ilango, G.P. Muthudevi, I. Prabha, R. Arthimhanju, Phytofabrication of selenium nanoparticles using *Azolla pinnata*: evaluation of catalytic properties in oxidation, antioxidant and antimicrobial activities, *J. Environ. Chem. Engin.* 9 (2021) 105483.
- A.K. Mittal, Y. Chisti, U.C. Banerjee, Synthesis of metallic nanoparticles using plant extracts, *Biotechnol. Adv.* 31 (2013) 346–356.
- C.S. Philip, A. Nivetha, C. Sakthivel, C. Veena, I. Prabha, Novel fabrication of cellulose sprinkled crystalline nanocomposites using economical fibrous sources: high performance, compatible catalytic and electrochemical properties, *Microp. Mesop. Mater.* 318 (2021) 111021.
- A. Nivetha, S.M. Devi, I. Prabha, Fascinating physic-chemical properties and resourceful applications of selected cadmium Nanomaterials, *J. Inorg. Organomet. Polym. Mater.* 29 (2019) 1423–1438.
- M.I. Din, R. Rehan, Synthesis, characterization, and applications of copper nanoparticles, *Anal. Lett.* 50 (2017) 50–62.
- I. Prabha, A. Nivetha, C. Sakthivel, Effective/comparative investigation on green mediated nano copper oxide: fabrication, characterization and environmental applications, *Mater. Today: Proceedings* (2020).
- M. Benguigui, I.S. Weitz, M. Timaner, T. Kan, D. Shechter, O. Perlman, et al., Copper oxide nanoparticles inhibit pancreatic tumor growth primarily by targeting tumor initiating cells, *Sci. Rep.* 9 (2019) 1–10.
- G. Benelli, Green synthesized nanoparticles in the fight against mosquito-borne diseases and cancer—a brief review, *Enzym. Microb. Technol.* 95 (2016) 58–68.
- T. Kayalvizhi, S. Ravikumar, P. Venkatachalam, Green synthesis of metallic silver nanoparticles using *Curculigo orchioides* rhizome extracts and evaluation of its antibacterial, larvicidal, and anticancer activity, *J. Environ. Eng.* 142 (2016), C4016002.
- S. Senthil-Nathan, A review of biopesticides and their mode of action against insect pests, *Environ. Sustain.* (2015) 49–63.
- P. Kaur, R. Thakur, A. Chaudhury, Biogenesis of copper nanoparticles using peel extract of *Punica granatum* and their antimicrobial activity against opportunistic pathogens, *Green Chem. Lett. Rev.* 9 (2016) 33–38.
- R. Khani, B. Roostaei, G. Bagherzade, M. Moudi, Green synthesis of copper nanoparticles by fruit extract of *Ziziphus spina-christi* (L.) Willd.: application for adsorption of triphenylmethane dye and antibacterial assay, *J. Mol. Liq.* 255 (2018) 541–549.
- S. Thakur, S. Sharma, S. Thakur, R. Rai, Green synthesis of copper nano-particles using *Asparagus adscendens* roxb. Root and leaf extract and their antimicrobial activities, *Int. J. Curr. Microbiol. Appl. Sci.* 7 (2018) 683–694.
- I.M. Chung, A. Abdul Rahuman, S. Marimuthu, A. Vishnu Kirthi, K. Anbarasan, P. Padmini, et al., Green synthesis of copper nanoparticles using *Eclipta prostrata* leaves extract and their antioxidant and cytotoxic activities, *Experim. Therap. Med.* 14 (2017) 18–24.
- M. Nasrollahzadeh, S.M. Sajadi, Green synthesis of copper nanoparticles using *Ginkgo biloba* L. leaf extract and their catalytic activity for the Huisgen [3+ 2] cycloaddition of azides and alkynes at room temperature, *J. Colloid Interface Sci.* 457 (2015) 141–147.
- R. Srivastava, A review on phytochemical, pharmacological, and pharmacognostical profile of *Wrightia tinctoria*: adulterant of kurchi, *Phcog. Rev.* 8 (2014) 36.
- S. Baskararaj, P. Theivendren, P. Palanisamy, S. Kannan, P. Pavadai, S. Arunachalam, et al., Optimization of bioactive compounds extraction assisted by microwave parameters from *Kappaphycus alvarezii* using RSM and ANFIS modeling, *J. Food Measur. Character.* 13 (2019) 2773–2789.
- I.Z. Luna, B.A.E. Commission, Preparation and characterization of copper oxide nanoparticles synthesized via chemical precipitation method, *Open Access Libr. J.* 2 (2015) 1.
- N. Pourreza, K. Ghanemi, Determination of copper by flame atomic absorption spectrometry after solid-phase extraction, *Spectrosc. Lett.* 39 (2006) 127–134.
- H. Iftikhar, S. Rashid, Molecular docking studies of flavonoids for their inhibition pattern against  $\beta$ -catenin and pharmacophore model generation from experimentally known flavonoids to fabricate more potent inhibitors for Wnt signaling pathway, *Phcog. Mag.* 10 (2014) S264.
- G. Chakraborty, J. Shin, Q.T. Nguyen, A. Harikishore, K. Baek, H.S. Yoon, Solution structure of FK506-binding protein 12 from *Aedes aegypti*, *Proteins: Struct. Funct. Bioinform.* 80 (2012) 2476–2481.
- U.P. Mohan, B. Sriram, T. Panneerselvam, S. Devaraj, D. MubarakAli, P. Parasuraman, et al., Utilization of plant-derived Myricetin molecule coupled with ultrasound for the synthesis of gold nanoparticles against breast cancer, *N. Schmied. Arch. Pharmacol.* 393 (2020) 1963–1976.
- S. Kunjiappan, M. Sankaranarayanan, B.K. Kumar, P. Pavadai, E. Babkiewicz, P. Maszcyk, et al., Capsaicin-loaded solid lipid nanoparticles: design, biodistribution, in silico modeling and in vitro cytotoxicity evaluation, *Nanotechnology* 32 (2020), 095101.
- S. Release, 3: Desmond Molecular Dynamics System, DE Shaw research, New York, NY, 2017. Maestro-Desmond Interoperability Tools, Schrödinger, New York, NY, 2017.
- W.L. Jorgensen, D.S. Maxwell, J. Tirado-Rives, Development and testing of the OPLS all-atom force field on conformational energetics and properties of organic liquids, *J. Am. Chem. Soc.* 118 (1996) 11225–11236.
- W.L. Jorgensen, J. Chandrasekhar, J.D. Madura, R.W. Impey, M.L. Klein, Comparison of simple potential functions for simulating liquid water, *J. Chem. Phys.* 79 (1983) 926–935.
- S. Nosé, A unified formulation of the constant temperature molecular dynamics methods, *J. Chem. Phys.* 81 (1984) 511–519.
- B.S. Hussain, P. Bethapudi, F.A. Rambabu Majji, NVS Viswanadha murthy M, Sreenivasa reddy E." Anti-angiogenesis property by Quercetin compound targeting VEGFR2 elucidated in a computational approach, *Europ. J. Biotech. Biosci.* 2 (2014) 30–46.
- H. Raja Naika, V. Krishna, K. Lingaraju, V. Chandramohan, M. Dammali, P. Navya, et al., Molecular docking and dynamic studies of bioactive compounds from *Naravelia zeylanica* (L.) DC against glycogen synthase kinase-3 $\beta$  protein, *J. Taibah Uni. Sci.* 9 (2015) 41–49.
- S. Kunjiappan, S. Govindaraj, P. Parasuraman, M. Sankaranarayanan, S. Arunachalam, P. Palanisamy, et al., Design, in silico modelling and

- functionality theory of folate-receptor-targeted myricetin-loaded bovine serum albumin nanoparticle formulation for cancer treatment, *Nanotechnology* 31 (2020) 155102.
- [32] G. Rajagopal, J. Jeyavani, S. Ilango, Larvicidal and histopathological efficacy of inhabitant pathogenic bacterial strains to reduce the dengue vector competence, *Pest Manag. Sci.* 76 (2020) 3587–3595.
- [33] G. Rajagopal, N. Manivannan, M. Sundararajan, A.G. Kumar, S. Senthilkumar, N. Mathivanan, et al., Biocompatibility assessment of silver chloride nanoparticles derived from *Padina gymnospora* and its therapeutic potential, *Nano Express* 2 (2021), 010010.
- [34] G. WHO, Report of the WHO Informal Consultation on the Evaluation and Testing of Insecticides, World Health Organization Geneva, 1996.
- [35] B.K. Sharma, D.V. Shah, D.R. Roy, Green synthesis of CuO nanoparticles using *Azadirachta indica* and its antibacterial activity for medicinal applications, *Mater. Res. Express* 5 (2018), 095033.
- [36] D. Kalaimurugan, P. Sivasankar, K. Lavanya, M.S. Shivakumar, S. Venkatesan, Antibacterial and larvicidal activity of *Fusarium proliferatum* (YNS2) whole cell biomass mediated copper nanoparticles, *J. Cluster Sci.* 30 (2019) 1071–1080.
- [37] A.Y. Ghidan, T.M. Al-Antary, A.M. Awwad, Green synthesis of copper oxide nanoparticles using *Punica granatum* peels extract: effect on green peach Aphid, *Environ. Nanotech. Monitor. Manag.* 6 (2016) 95–98.
- [38] D.R. Preeth, M. Shairam, N. Suganya, R. Hootan, R. Kartik, K. Pierre, et al., Green synthesis of copper oxide nanoparticles using sinapic acid: an underpinning step towards antiangiogenic therapy for breast cancer, *JBIC J. Biol. Inorg. Chem.* 24 (2019) 633–645.
- [39] M.K. Ghosh, S. Sahu, I. Gupta, T.K. Ghorai, Green synthesis of copper nanoparticles from an extract of *Jatropha curcas* leaves: characterization, optical properties, CT-DNA binding and photocatalytic activity, *RSC Adv.* 10 (2020) 22027–22035.
- [40] P. Mulvaney, Surface plasmon spectroscopy of nanosized metal particles, *Langmuir* 12 (1996) 788–800.
- [41] M. Nasrollahzadeh, S.M. Sajadi, A. Rostami-Vartooni, S.M. Hussin, Green synthesis of CuO nanoparticles using aqueous extract of *Thymus vulgaris* L. leaves and their catalytic performance for N-arylation of indoles and amines, *J. Colloid Interface Sci.* 466 (2016) 113–119.
- [42] N.A. Alomair, H.H. Mohamed, Green synthesis of ZnO hollow microspheres and ZnO/rGO nanocomposite using red rice husk extract and their photocatalytic performance, *Mater. Res. Express* 5 (2018), 095012.
- [43] M.A. Alsaheb, S.A. Alsaheb, Synthesis, characterization and polymerization of 1Hpyrazolo [1, 2-b] phthalazine-5, 10-dione derivatives using CuO nanoparticle oxide from natural source as catalyst, *Drug Deliv.* 10 (2020) 530–536.
- [44] S. Hane, A. Sharma, M. Dhaygude, S. Joglekar, K. Kodam, M. Hudlikar, Novel route for rapid biosynthesis of copper nanoparticles using aqueous extract of *Calotropis procera* L. latex and their cytotoxicity on tumor cells, *Colloids Surf. B Biointerfaces* 95 (2012) 284–288.
- [45] F. Soofivand, M. Salavati-Niasari, Novel solvent-less synthesis of CuO nanoparticles by using sublimated precursors, *Mater. Lett.* 106 (2013) 83–86.
- [46] M.-H. Youn, Y.-M. Lim, H.-J. Gwon, J.-S. Park, S.-J. An, Y.-C. Nho, Characterization of an antibacterial silver chloride/poly (acrylic acid) deodorant prepared by a gamma-ray irradiation, *Macromol. Res.* 17 (2009) 813–816.
- [47] S. Balakrishnan, M. Srinivasan, J. Mohanraj, Biosynthesis of silver nanoparticles from mangrove plant (*Avicennia marina*) extract and their potential mosquito larvicidal property, *J. Parasit. Dis.* 40 (2016) 991–996.
- [48] E.A. Sharon, K. Velayutham, R. Ramanibai, Biosynthesis of copper nanoparticles using *Artocarpus heterophyllus* against dengue vector *Aedes aegypti*, *Int J Life Sci Scienti Res eISSN* 2455 (2018) 1716.
- [49] J. Karimi, S. Mohsenzadeh, Rapid, green, and eco-friendly biosynthesis of copper nanoparticles using flower extract of *Aloe vera*. *Synthesis and Reactivity in Inorganic, Metal-Organic, Nano-Metal Chemistry* 45 (2015) 895–898.
- [50] A. Azam, A.S. Ahmed, M. Oves, M.S. Khan, S.S. Habib, A. Memic, Antimicrobial activity of metal oxide nanoparticles against Gram-positive and Gram-negative bacteria: a comparative study, *Int. J. Nanomed.* 7 (2012) 6003.
- [51] R. Sivaraj, P.K. Rahman, P. Rajiv, H.A. Salam, R. Venckatesh, Biogenic copper oxide nanoparticles synthesis using *Tabernaemontana divaricate* leaf extract and its antibacterial activity against urinary tract pathogen, *Spectrochim. Acta Mol. Biomol. Spectrosc.* 133 (2014) 178–181.
- [52] C. Santini, M. Pellei, V. Gandin, M. Porchia, F. Tisato, C. Marzano, Advances in copper complexes as anticancer agents, *Chem. Rev.* 114 (2014) 815–862.
- [53] G. Mendoza-Diaz, R. Garcia-Nieto, I. Gracia-Mora, S. Arias-Negrete, L. Ruiz-Ramirez, I. Cosenza, et al., Synthesis, characterization and biological activity of some mixed complexes of Cu (II) and Zn (II) with antibiotics of the nalidixic acid family and N N ligands, *J. Inorg. Biochem.* 43 (1991) 640.
- [54] O.I. Aruoma, B. Halliwell, E. Gajewski, M. Dizdaroglu, Copper-ion-dependent damage to the bases in DNA in the presence of hydrogen peroxide, *Biochem. J.* 273 (1991) 601–604.
- [55] S.M. Selvan, K.V. Anand, K. Govindaraju, S. Tamilselvan, V.G. Kumar, K.S. Subramanian, et al., Green synthesis of copper oxide nanoparticles and mosquito larvicidal activity against dengue, zika and chikungunya causing vector *Aedes aegypti*, *IET Nanobiotechnol.* 12 (2018) 1042–1046.
- [56] M. Abinaya, B. Vaseeharan, R. Rekha, S. Shanthini, M. Govindarajan, N.S. Alharbi, et al., Microbial exopolymer-capped selenium nanowires—Towards new antibacterial, antibiofilm and arbovirus vector larvicides? *J. Photochem. Photobiol. B Biol.* 192 (2019) 55–67.
- [57] G. Benelli, Mode of action of nanoparticles against insects, *Environ. Sci. Pollut. Control Ser.* 25 (2018) 12329–12341.
- [58] J. Choi, V. Reipa, V.M. Hitchins, P.L. Goering, R.A. Malinauskas, Physicochemical characterization and *in vitro* hemolysis evaluation of silver nanoparticles, *Toxicol. Sci.* 123 (2011) 133–143.
- [59] S. Libi, B. Calenic, C.E. Astete, C. Kumar, C.M. Sabliov, Investigation on hemolytic effect of poly (lactic co-glycolic) acid nanoparticles synthesized using continuous flow and batch processes, *Nanotechnol. Rev.* 6 (2017) 209–220.
- [60] P. AshaRani, G. Low Kah Mun, M.P. Hande, S. Valiyaveetil, Cytotoxicity and genotoxicity of silver nanoparticles in human cells, *ACS Nano* 3 (2009) 279–290.